Electron Paramagnetic Resonance Imaging and Spectroscopy of Polydopamine Radicals

ARTICLE *in* THE JOURNAL OF PHYSICAL CHEMISTRY B · JULY 2015

Impact Factor: 3.3 · DOI: 10.1021/acs.jpcb.5b01524

THE JOURNAL OF PHYSICAL CHEMISTRY B

Article

pubs.acs.org/JPCB

Electron Paramagnetic Resonance Imaging and Spectroscopy of Polydopamine Radicals

Radosław Mrówczyński,[†] L. Emerson Coy,[†] Błażej Scheibe,[†] Tomasz Czechowski,[†] Maria Augustyniak-Jabłokow,[‡] Stefan Jurga,[†] and Krzysztof Tadyszak*[,†]

[†]NanoBioMedical Centre, Adam Mickiewicz University, ul. Umultowska 85, 61614 Poznań, Poland

[‡]Institute of Molecular Physics, Polish Academy of Sciences, ul. Mariana Smoluchowskiego 17, 60179 Poznań, Poland

ABSTRACT: A thorough investigation of biomimetic polydopamine (PDA) by Electron Paramagnetic Resonance (EPR) is shown. In addition, temperature dependent spectroscopic EPR data are presented in the range 3.8−300 K. Small discrepancies in magnetic susceptibility behavior are observed between previously reported melanin samples. These variations were attributed to thermally acitivated processes. More importantly, EPR spatial−spatial 2D imaging of polydopamine radicals on a phantom is presented for the first time. In consequence, a new possible application of polydopamine as EPR imagining marker is addressed.

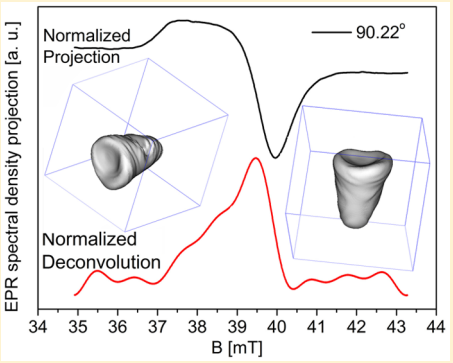

INTRODUCTION

Polymer chemistry and material science have grown significantly in the last years. Progress done in these fields has stimulated also other areas, i.e., nanotechnology, organic coatings, and medicine. Coatings play a key role in preparation of biomedical materials; thus, there are some conditions that need to be fulfilled by the applied coating agent. It needs to be nontoxic, biocompatible, and easily available. Recently, inspiration for synthesis of such a polymer was taken from nature by Messersmith.[1−3] Structural investigation of one of the proteins Mefp-5 responsible for adhesive properties of mussel revealed that it is reached in L-3,4-dihydroxyphenylalanine (L-DOPA).[4] Research on oxidative polymerization of structurally similar dopamine led to the development of polydopamine (PDA).[5−7] This new polymer was found to be nontoxic and biocompatible.[8] Because of its unique properties and simple preparation method polydopamine has found wide application in coating magnetic nanoparticles,[9] immobilization of growth factors,[10] enzyme,s[11,12] and biomolecules[13] on various supports and modification scaffold for tissue engineering.[14] The biomedical application include also synthesis of antibacterial[15] and drug delivery systems.[16] It has been demonstrated that PDA can bear radicals in the structure and possesses a free-radical-scavenging property.[17] In addition, it exhibits strong adhesive properties toward myriad materials, i.e., Teflon, wood, stainless steel, polylactic acid, silica, iron oxides, aluminum oxide, and noble metals (Au, Ag, Pt, Pd).[3,18−20] Polydopamine covered materials are obtained by polymerization of dopamine using dip method under air access. Although, its structure is still under discussion, there is a consensus that it is built up of indole units of different states of hydrogenation, mainly connected by C−C bonds between the benzene rings.[21] Nevertheless, other structures were proposed which point for heterogeneity of the PDA.[22,23]

Electron paramagnetic resonance (EPR) is one of the most common methods in biomedical applications because of its versatility and sensitivity. EPR is capable of detecting free radicals as well as transition and rare-earth ions and has found numerous applications in biology,[24] chemistry,[25] physics,[26] and medicine.[27−30] The EPR spectrum provides a wealth of information about the molecular structure of the paramagnetic species as well as its local environment.

Over the past four decades, EPR-based imaging (EPRI) has been used to observe the distribution of free radicals in biological systems[31] and further to study the oxygen content in tissues (EPR-oximetry).[32] The advantage of the EPR technique is the possibility of distinguishing between different types of radicals, their number, and radical scavenging effects of different substances.[33−36] The extension of the methods mentioned above reaches single electron spin resonance by applying optical detection methods,[37] subcellular structure imaging,[38,39] and nanodiamonds imaging.[40]

Even though PDA is a versatile polymer with proven radical structures, the detailed spectroscopic EPR analysis and EPR imaging of polydopamine has not been presented to date. In this work we present profound EPR research and EPR imaging investigations on polydopamine. Moreover, characterization of radical behavior of polydopamine at different temperatures is described. Obtained results are of tremendous importance in many fields such as biology, chemistry, and medicine, where

Received: February 13, 2015
Revised: July 15, 2015
Published: July 15, 2015

DOI: 10.1021/acs.jpcb.5b01524
J. Phys. Chem. B 2015, 119, 10341−10347

PDA is used as coating material or part of complex nanocomposites.

EXPERIMENTAL SECTION

Dopamine hydrochloride and tris (hydroxymethyl)-aminomethane (TRIS) were purchased from Alfa Aesar and used without any purification. For polymerization reaction Milli-Q deionized water (resistivity 18 MΩ·cm) was used.

Dopamine hydrochloride (1 g, 5.3 mmol) was dissolved in 500 mL of 10 mM buffer (TRIS pH = 8.5 and phosphate pH = 8.5) and stirred under air for 24 h. The resulting black precipitate was separated by centrifugation, washed with water, and centrifuged again. This washing step was repeated three times and the solid was dried at 50 °C overnight.

From the TRIS buffer we got a sample containing 17% wt of H_2O and from phosphate buffer 8.2% wt and 0% wt of H_2O. The last sample was gained after 6 h of outgassing (10^{-7} hPa) and silling in quartz tube after that.

Transmission electron microscopy (TEM) images were recorded on a JEM-1400 microscope made by JEOL (Japan). The accelerating voltage was 120 kV. A small amount of the sample, placed on a copper measuring grid (Formvar/Carbon 200 Mesh made by TedPella (USA)) after 5 min of sonication in deionized water. Then the sample was dried in a vacuum desiccator for 24 h.

FTIR spectra were recorded on Bruker Tensor 27 spectrometer in KBr pallets

Imaging experiments were conducted with E 540 L-Band imaging spectrometer equipped with E 540R23 L-Band EPR-Resonator) at room temperature, 23 °C. The mass of the sample was 110 mg. The polydopamine sample was imaged in a Nunc 15 mL conical sterile polypropylene centrifuge tube. Spectra for imaging were recorded in the field range 34.9−43.3 mT, 2048 points, and field sweep 8.35 mT with center at 39.098 mT. Entire, 2D reconstruction demanded 402 projections, whereas over 6000 were used for 3D. The first angle to external magnetic field axes was of 0.223° and last 179.776°. Scans were accumulated five times. Microwave power was set 22.7 mW (no saturation effects appeared). Frequency was 1.09×10^9 Hz, modulation amplitude 0.1 mT (100 kHz), sampling time 10 ms, gradient strength 30 G/cm (for both 2D and 3D).

The spectroscopic EPR measurements were performed on a RADIOPAN SX spectrometer with an Oxford CF935 cryostat allowing measurements in the temperature range 4.2−300 K. The modulation amplitude was 0.05 mT, the microwave power was 11.38 mW (without saturation effects), and the microwave frequency was recalculated for each measured point to exact 9 GHz. The number of points per spectra was 1024, accumulations 2, time per one point 120 ms (4.2 K) to 520 ms (300 K).

RESULTS AND DISCUSSION

Polydopamine was synthesized using previously described procedure.[21] The reaction was performed in TRIS buffer in an open vessel. The mass of obtained black precipitate was slightly above 300 mg, which was used in all further experiments. To determine the morphology of the sample, the TEM analysis was performed (Figure 1). The polymer particles were spherical in shape but slightly aggregated. This is attributed to two main factors. First, the aggregation is promoted by the sample preparation process, specifically by the overnight drying and the interaction between polydopamine particles at that stage. Second, the dospherical shape of particles with well-defined boundaries suggests that the aggregation process takes place at later stages of the synthesis, after the initial particles were already formed. Nevertheless, slight aggregation of PDA particles is not uncommon in the literature.[41,42]

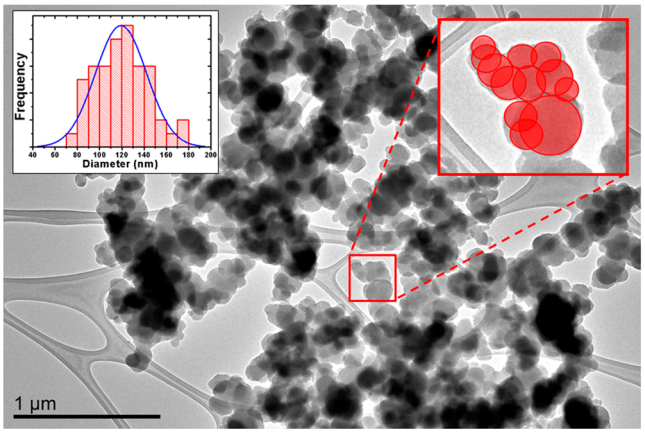

Figure 1. TEM image of polydopamine with size distribution. Red spheres represent the area fitted for each particle.

Statistical analysis of several TEM micrographs allowed the extraction of particle size distribution for the sample. This process was performed by allocating pseudospherical areas on each particle and measuring their estimated diameter. Values are showed in the shape of a histogram (Figure 1, inset). The histogram describes a pseudonormal distribution with a skewness of 0.22, showing that the distribution is slightly weighted to the right side of the histogram, a normal behavior in synthesized nanoparticles. The standard deviation is found to be 23 nm, and the mean value 119 nm showing a rather narrow size distribution.

Freshly prepared polydopamine powder was mixed with KBr powder to form a pellet and analyzed in FT-IR (Figure 2). The

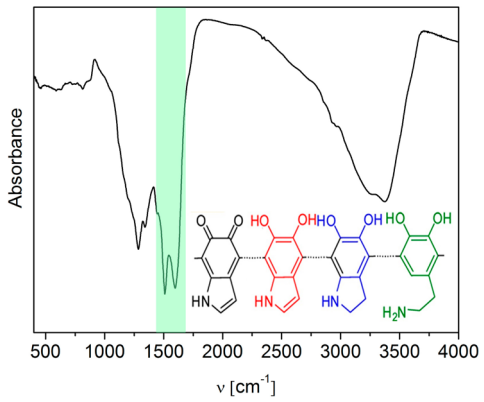

Figure 2. Infrared absorption spectrum of polydopamine in KBr pellet. The inset shows theoretical polydopamine structure.

FTIR spectrum was in agreement with previously reported data.[21] Signals in the range 1500−1600 cm^{-1} are assigned to the various N−H vibrations. The broad peak spanning 3200−3500 cm^{-1} is due to the presence of hydroxyl structures as well as water. The expected signal from carbonyl group is not observed in this spectrum. The structure of polydopamine is not obvious. The inset shows only basic groups but not all

DOI: 10.1021/acs.jpcb.5b01524
J. Phys. Chem. B 2015, 119, 10341−10347

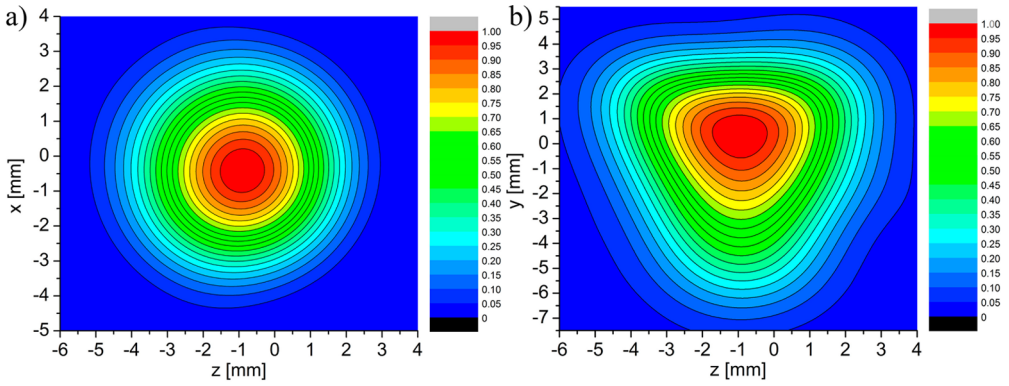

Figure 3. 2D spatial−spatial reconstruction of the sample in (a) *xz* and (b) *yz* planes.

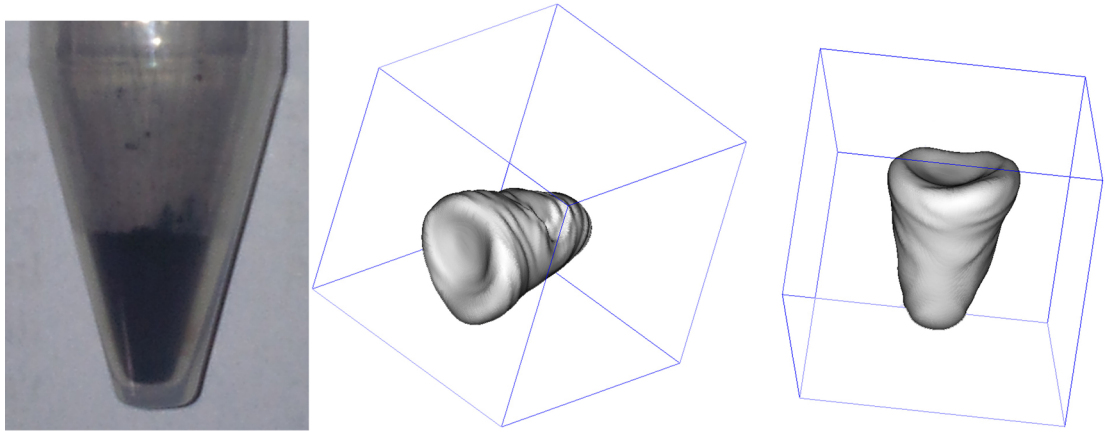

Figure 4. Polydopamine powder sample squeezed in a 15 mL polystyrene tube; 3D EPRI spatial−spatial reconstruction of the sample (Image Viewer 1.5).

possible alleged combinations.[21] The sample obtained in phosphate buffer gave an identical absorption spectrum.

IMAGING

Polydopamine has been proved to have radical structure similarly to naturally occurring melanins.[43] It has been widely used in various biomedical applications and even in vivo studies.[44] Nevertheless, according to the best of our knowledge EPR imagining has not been performed on emulamine or polydopamine, despite its wide applicability and radical rich structure. Thus, we decided to investigate the possibility of using polydopamine as EPR imaging marker.

Standard EPR imaging in continuous wave (CW) mode uses a magnetic field gradient that is constant during sweep time. After each measurement, gradient orientation rotates by a fixed angle depending on the number of projections, whose orientations are equally distributed in the polar coordinate system within the 0−180° range for 2D imaging. By acquiring a number of projections along different directions, a two- or three-dimensional image can be obtained depending on gradient orientations schemes. The image obtained by the method only represented the spatial distribution of the free radicals, without providing any spectral information, e.g., line shape, line width. To obtain data about the surroundings of the free radicals, it was necessary to acquire information not only about the spatial but also about the spectral distribution. For this purpose, an additional spectral-spatial imaging technique was used for each projection separately as reported previously.[45,46]

As a result, the measured data in the presence of a static magnetic field gradient were the spin density projections, convoluted with the nongradient EPR spectrum. Raw data were obtained by sweeping the magnetic field for a collection selected gradient angles ($grad_{\alpha}(B)$ = const) lying on the projection surface. The result of the imaging experiment was the function expressed here as a convolution. The spatial distribution of spin density was coded within this function. Necessary spin density function was obtained by deconvolution of raw data. This was done in both frequency and time domains.[47] In this study the deconvolution was performed by filtered Fourier transformation of the raw projections data and reference spectrum preceding inverse Fourier transformation of theirs quotient. The signal was filtered before the inverse Fourier transform to remove the high frequency noise signal in the frequency domain. After deconvolution, the raw data were converted into a sinogram, which contains all information needed to reconstruct the image of polydopamine particles.

The reconstruction of 2D and 3D images was done by a filtered back-projection method. This method utilizes inverse radon transformation. Reconstructed images are depicted in Figure 3a,b.

Reconstructed images represent a spread of unpaired electron spins in the sample. The observed images (Figure 3) are the sum of all parallel slices to the "*xz*" horizontal plane, where "*z*" is the direction of the external magnetic field and "*x*" axis is perpendicualar to "*z*" and to the resonator axis (*y*). The "*yz*" vertical plane is spanned between the resonator axis and the direction of the external magnetic field. A right-handed axis

DOI: 10.1021/acs.jpcb.5b01524
J. Phys. Chem. B 2015, 119, 10341−10347

system is used. The powder sample in the tube had the height of about 11 mm and a maximal diameter of 8 mm. Three-dimensional reconstructions and a photograph of the sample are depicted in Figure 4. The visible wrinkles after the reconstruction are the result of imperfections of the squeezing polydopamine in the tube.

SPECTROSCOPY

The oxidative polymerization process of dopamine is heterogeneous, resulting in a high order of randomness. Mass spectrometry data roughly estimate the molecular mass in the range between 140 and 200 g/mol,[48] for example, 150.15 g mol^{-1}.[23] Reported values can change depending on applied conditions, i.e., time, dopamine concentration, and buffer. We decided to examine deeply the radical structure of polydopamine by solid state electron paramagnetic resonance (EPR) spectroscopy. Spectroscopic results gained for polydopamine samples are in equilibrium with atmospheric moisture. Broad-field EPR scans performed in helium temperatures showed no magnetic ordering, which could result in the appearance of new broad lines with different g values, and no contamination with metallic ions, having unapired spins.

The number of spins in the sample was determined by a comparison with ten fresh prepared $CuSO_4 \cdot 5H_2O$ monocrystals of different weights.[49,50] A simultaneous comparison method was used, and the average value is reported while microwave line saturation was continuously monitored. The weight of polydopamine sample was 78 mg and the estimated number of spins from EPR measurements corresponds to 1.9×10^{17} spins (2.4×10^{15} spins/mg, 17% of moisture, L-band). Sample prepared in a different synthesis also from TRIS buffer, having 8.2% moisture, had 3.8×10^{15} spins/mg (3.6 mg of sample was measured, X-band), and sample prepared from phosphate buffer had 3.2×10^{15} spins/mg (10.2 mg of sample was measured, X-band). Results are comparable with values gained by Bielawski, 2.8×10^{15} spins/mg.[23] The amount of moisture was measured by weighting the sample before and after heating for at least 1 h in 100 °C. No difference in spin number was detected due to the measurement uncertainty of 30−50%.

If we agree after Bielawski that the molecular weight of polydopamine is around 150.15 g/mol, then unpaired electron spins appear not less than 1 on 1672 atoms of polydopamine, which can suggest that if they are homogeneously spread they do not interfere with each other by dipol−dipol and exchange interactions.

The integral intensity of polydopamine radicals taken from EPR measurements is proportional to magnetic susceptibility (Figure 5). In systems where magnetic dipole moments ($S = {}^1/_2$) are not interacting, the result follows the normalized Curie function ($\chi = C/T$ amplitude is 1 in 300 K and 79 in 3.8 K). It is shown that the susceptibility grows slower with the decreasing temperature than the Curie function predicts. At 3.8 K it is 6 times higher than at 300 K, when the expected increase is of 79 times. The microwave line saturation and temperature forced resonator changes were rejected as the cause in the first place. The sample was measured in ambient conditions while still having 17% of moisture after the synthesis (TRIS buffer). The results observed for natural and synthetic melanin reported in the work of Blois[48] indicate that the magnetic susceptibility obeys the Curie low in broad temperature range. Our results are similar to those obtained by Skrzypek,[51] where magnetic susceptibility is weakly dependent

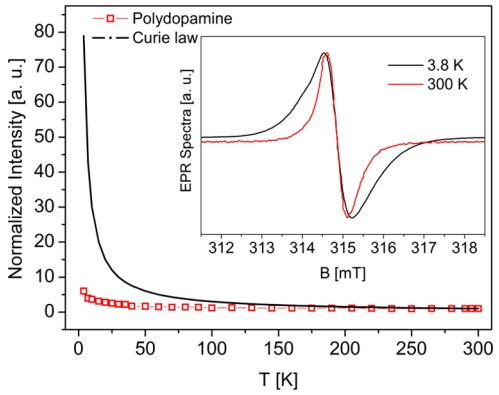

Figure 5. Normalized integral intensity of polydopamine (red squares, TRIS buffer 17% wt H_2O), normalized Curie line (black line). Inset: EPR lines of polydopamine recorded at 3.8 and 300 K.

on temperature. This behavior was explained by the appearance of thermally activated radicals. To study this behavior, we prepared fresh polydopamine from phosphate buffer containing 8.2% and 0% of moisture. The magnetic susceptibility, which is proportional to integral intensity in the case of paramagnetic noninteracting particles, can be described by $I \sim \chi = M/H = Ng^2\beta^2/4k_BT$, where N is the number of spins, g is the spectroscopic g-factor, β is the Bohr magneton, k_B is the Boltzmann factor, and T is the temperature. In the case of thermally activated number of spins N is a function of temperature and can be described $N = N_0 \exp(E_{act}/k_BT)$, where E_{act} is the activation energy. Together it gives $IT \sim N_0 \exp(E_{act}/k_BT)g^2\beta^2/4k_B$ and after logarithm the equation takes the form $\ln(IT) \sim \ln(N_0g^2\beta^2/4k_B) + E_{act}/k_BT = C_1 + 1/TC_2$.

Plotting the natural logaritm of the product of the integral intensity and temperature vs the reciprocal temperature gives the possibility to distinguish if the spin system fulfills the Arrhenius relation. It is shown in Figure 6 that the

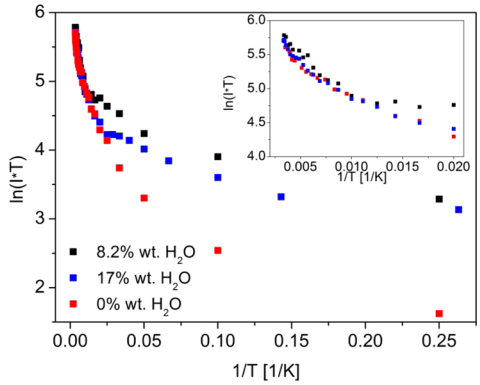

Figure 6. Natural logarithm of integral intensity times temperature vs reciprocal temperature. The inset shows magnification of the 0−0.03 region (TRIS buffer 17% wt H_2O, phosphate buffer 8.2% and 0% wt H_2O).

polydopamine sytem does not fulfill the Arrhenius relation and beyond that there are visible differences between water-containing samples and dry samples at low temperatures, if comparing PDA made out of phosphate buffer. The differences between PDA samples having 8.2% wt (phosphate buffer) and 17% wt are more visible if comparing their g-factors, which at room temperature are 2.0038 and 2.0052, respectively. That

DOI: 10.1021/acs.jpcb.5b01524
J. Phys. Chem. B 2015, 119, 10341−10347

means that the electronic structure of the polymer is slightly different in the place of the radical localization.

The inset in Figure 5 shows two normalized EPR lines of polydopamine (TRIS buffer 17% wt H_2O) recorded at 3.8 K (line width 0.68 mT) and 300 K (line width 0.52 mT). It can be seen that *g*-factors and the line shapes are different in both cases, composed of multiple components with very weak unresolved *g*-factor anisotropy The exact *g*-factor measurements were carried on with Cr^{5+} doped K_3NbO_8 crystal standards (Figure 7).[52] The *g*-factor measurements were done simultaneously after mixing polidopamine with powdered standard at room temperature. After that procedure, *g*-values measured in the full temperature range could be corrected. Previously measured *g*-values for melanins estimated the *g*-factor of the order 2.004,[42] which is lower from our value of 2.0052. The changes can arise from different *g* standards or sample related steaming from different amounts of moisture in the sample.

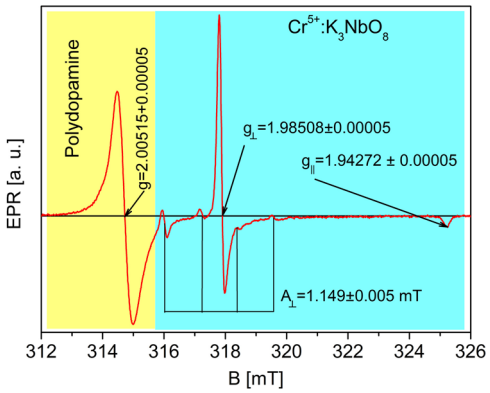

Figure 7. EPR spectra of polydopamine (marked with yellow area, TRIS buffer 17% wt H_2O) and Cr^{5+}:K_3NbO_8 *g*-factor standard (marked with aquamarine area).

The *g*-factor is constant in the full temperature range (~2.0052 ± 0.00005). A sample having 8.2% moisture (phosphate buffer) exhibits a *g* of about 2.0038 ± 0.00005. The line width is narrowest at room temperatures, 0.52 mT, and at 3.8 K it broadens to 0.68 mT. The outgassed sample resembles a similar temperature line width dependence starting from a line width of 0.53 mT at room temperature. The EPR line of PDA powder possessing natural moisture content (17%, inset, Figure 8) can be saturated below 11.38 mW at temperature 3.8 K whereas the outgassed and sealed PDA (TRIS buffer) saturates easily below 70 K (results not published). The line broadening at liquid helium temperatures is caused by the enhancement of the relaxation rate. The mechanism that leads to this effect is unknown. It is clear that further pulse EPR studies should be performed for estimating how the spin−lattice T_1, spin−spin T_2, and phase memory time T_M affect the line broadening.

CONCLUSIONS

Because of the radical nature of polydopamine EPR imaging could be successfully performed. As a result, 2D and 3D imaging of polydopamine phantom is demonstrated. The EPR imaging experiment performed on polydopamine showed the spin distribution that corresponds exactly to the photographed sample, which means that there are no regions with no unpaired spins. In light of the presented results, we postulate that polydopamine can be applied as a potential imaging marker for biomedical applications. For example, EPR imaging of polydopamine composites or coated structures seems to be possible.

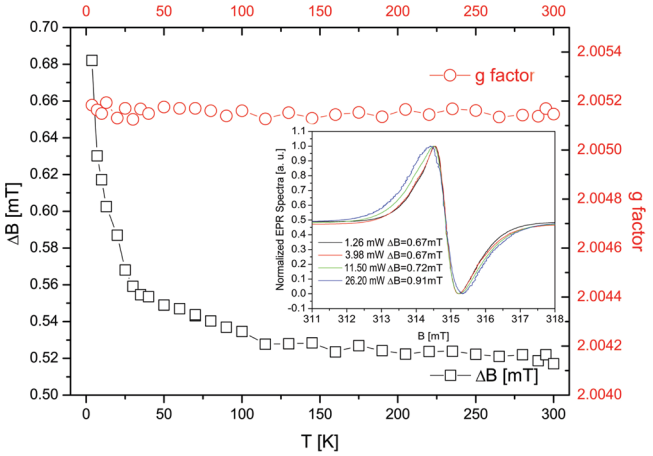

Figure 8. Integral intensity of polydopamine EPR signal measured in the temperature range 4.2−300 K. Lines connecting points are only guidelines for eye. Inset: saturation of signal observed at 3.8 K 1.26 and 3.98 mW corresponds to line width of 0.67 mT, 11.50 mW to 0.72 mT, 26.20 mW to 0.91 mT.

The spectroscopic data show one unresolved signal with a slightly asymmetrical line in the full temperature range. The temperature integral intensity behavior implys a thermal activation process, but the Arrhenius mechanism is not fulfilled. Beyond that, the amount of moisture in the sample plays a significant role in this behavior. The *g*-factor was determined to be ~2.0052 (17% wt of H_2O TRIS buffer) and is constant in a broad range of temperatures and for 8.2% wt of H_2O in phosphate buffer is ~2.0038 and slightly dropping below 100 K. Both the moisture content and the type of buffer used have an influence on the spectral parameters. This field requires further development and research on both the nature of polydopamine complexes and its effect on EPR imaging.

AUTHOR INFORMATION

Corresponding Author

*K. Tadyszak. E-mail: krztad@amu.edu.pl.

Notes

The authors declare no competing financial interest.

ACKNOWLEDGMENTS

Financial support from the National Centre for Research and Development contract number PBS1/A9/13/2012, and from the National Science Centre under project number UMO-2014/13/D/ST5/02793 is gratefully acknowledged.

REFERENCES

(1) Rivera, J. G.; Messersmith, P. B. Polydopamine-assisted Immobilization of Trypsin onto Monolithic Structures for Protein Digestion. *J. Sep. Sci.* **2012**, *35*, 1514−1520.

(2) Sileika, T. S.; Kim, H.-D.; Maniak, P.; Messersmith, P. B. Antibacterial Performance of Polydopamine-Modified Polymer Surfaces Containing Passive and Active Components. *ACS Appl. Mater. Interfaces* **2011**, *3*, 4602−4610.

(3) Lee, H.; Lee, B. P.; Messersmith, P. B. A reversible Wet/Dry Adhesive Inspired by Mussels and Geckos. *Nature* **2007**, *448*, 338−341.

(4) Waite, J. H.; Qin, X. Polyphosphoprotein From the Adhesive Pads of Mytilus Edulis. *Biochemistry* **2001**, *40*, 2887−2893.

DOI: 10.1021/acs.jpcb.5b01524
J. Phys. Chem. B 2015, 119, 10341−10347

(5) Liu, Y.; Ai, K.; Lu, L. Polydopamine and Its Derivative Materials: Synthesis and Promising Applications in Energy, Environmental, and Biomedical Fields. *Chem. Rev.* **2014**, *114*, 5057−5115.
(6) Lynge, M. E.; van der Westen, R.; Postma, A.; Stadler, B. Polydopamine-a Nature-Inspired Polymer Coating for Biomedical Science. *Nanoscale* **2011**, *3*, 4916−4928.
(7) Dreyer, D. R.; Miller, D. J.; Freeman, B. D.; Paul, D. R.; Bielawski, C. W. Perspectives on Poly(dopamine). *Chem.Sci.* **2013**, *4*, 3796−3802.
(8) Liu, X.; Cao, J.; Li, H.; Li, J.; Jin, Q.; Ren, K.; Ji, J. Mussel-Inspired Polydopamine: A Biocompatible and Ultrastable Coating for Nanoparticles in Vivo. *ACS Nano* **2013**, *7*, 9384−9395.
(9) Martin, M.; Salazar, P.; Villalonga, R.; Campuzano, S.; Pingarron, J. M.; Gonzalez-Mora, J. L. Preparation of Core-Shell Fe3O4@ poly(dopamine) Magnetic Nanoparticles for Biosensor Construction. *J. Mater. Chem. B* **2014**, *2*, 739−746.
(10) Shin, Y. M.; Lee, Y. B.; Kim, S. J.; Kang, J. K.; Park, J.-C.; Jang, W.; Shin, H. Mussel-Inspired Immobilization of Vascular Endothelial Growth Factor (VEGF) for Enhanced Endothelialization of Vascular Grafts. *Biomacromolecules* **2012**, *13*, 2020−2028.
(11) Ren, Y.; Rivera, J.; He, L.; Kulkarni, H.; Lee, D.-K.; Messersmith, P. Facile, High Efficiency Immobilization of Lipase Enzyme on Magnetic Iron Oxide Nanoparticles via a Biomimetic Coating. *BMC Biotechnol.* **2011**, *11*, 63.
(12) Gao, X.; Ni, K.; Zhao, C.; Ren, Y.; Wei, D. Enhancement of the Activity of Enzyme Immobilized on Polydopamine-Coated Iron Oxide Nanoparticles by Rational Orientation of Formate Dehydrogenase. *J. Biotechnol.* **2014**, *188*, 36−41.
(13) Lee, H.; Rho, J.; Messersmith, P. B. Facile Conjugation of Biomolecules onto Surfaces via Mussel Adhesive Protein Inspired Coatings. *Adv. Mater.* **2009**, *21*, 431−434.
(14) Tsai, W.-B.; Chen, W.-T.; Chien, H.-W.; Kuo, W.-H.; Wang, M.-J. Poly(dopamine) Coating of Scaffolds for Articular Cartilage Tissue Engineering. *Acta Biomater.* **2011**, *7*, 4187−4194.
(15) Shalev, T.; Gopin, A.; Bauer, M.; Stark, R. W.; Rahimipour, S. Non-Leaching Antimicrobial Surfaces Through Polydopamine Bio-inspired Coating of Quaternary Ammonium Salts or An Ultrashort Antimicrobial Lipopeptide. *J. Mater. Chem.* **2012**, *22*, 2026−2032.
(16) Cui, J.; Yan, Y.; Such, G. K.; Liang, K.; Ochs, C. J.; Postma, A.; Caruso, F. Immobilization and Intracellular Delivery of An Anticancer Drug Using Mussel-Inspired Polydopamine Capsules. *Biomacromolecules* **2012**, *13*, 2225−2228.
(17) Ju, K.-Y.; Lee, Y.; Lee, S.; Park, S. B.; Lee, J.-K. Bioinspired Polymerization of Dopamine to Generate Melanin-Like Nanoparticles Having an Excellent Free-Radical-Scavenging Property. *Biomacromolecules* **2011**, *12*, 625−632.
(18) Mrówczyński, R.; Turcu, R.; Leostean, C.; Scheidt, H. A.; Liebscher, J. New Versatile Polydopamine Coated Functionalized Magnetic Nanoparticles. *Mater. Chem. Phys.* **2013**, *138*, 295−302.
(19) Cont, L.; Grant, D.; Scotchford, C.; Todea, M.; Popa, C. Composite PLA Scaffolds Reinforced with PDO Fibers for Tissue Engineering. *J. Biomater. Appl.* **2013**, *27*, 707−716.
(20) Luo, R.; Tang, L.; Wang, J.; Zhao, Y.; Tu, Q.; Weng, Y.; Shen, R.; Huang, N. Improved Immobilization of Biomolecules to Quinone-Rich Polydopamine for Efficient Surface Functionalization. *Colloids Surf., B* **2013**, *106*, 66−73.
(21) Liebscher, J.; Mrówczyński, R.; Scheidt, H. A.; Filip, C.; Hădade, N. D.; Turcu, R.; Bende, A.; Beck, S. Structure of Polydopamine: A Never-Ending Story? *Langmuir* **2013**, *29*, 10539−10548.
(22) Yu, X.; Fan, H.; Liu, Y.; Shi, Z.; Jin, Z. Characterization of Carbonized Polydopamine Nanoparticles Suggests Ordered Supramolecular Structure of Polydopamine. *Langmuir* **2014**, *30*, 5497−5505.
(23) Dreyer, D. R.; Miller, D. J.; Freeman, B. D.; Paul, D. R.; Bielawski, C. W. Elucidating the Structure of Poly(dopamine). *Langmuir* **2012**, *28*, 6428−6435.
(24) Fujii, H. G.; Sato-Akaba, H.; Emoto, M. C.; Itoh, K.; Ishihara, Y.; Hirata, H. Noninvasive Mapping of The Redox Status in Septic Mouse by In Vivo Electron Paramagnetic Resonance Imaging. *Magn. Reson. Imaging* **2013**, *31*, 130−138.
(25) Tresp, H.; Hammer, M. U.; Winter, J.; Weltmann, K.-D.; Reuter, S. Quantitative Detection of Plasma-Generated Radicals in Liquids by Electron Paramagnetic Resonance Spectroscopy. *J. Phys. D: Appl. Phys.* **2013**, *46*, 435401.
(26) Chiesa, M.; Paganini, M. C.; Livraghi, S.; Giamello, E. Charge Trapping in TiO2 Polymorphs as Seen by Electron Paramagnetic Resonance Spectroscopy. *Phys. Chem. Chem. Phys.* **2013**, *15*, 9435−9447.
(27) Presley, T.; Kuppusamy, P.; Zweier, J. L.; Ilangovan, G. Electron Paramagnetic Resonance Oximetry as a Quantitative Method to Measure Cellular Respiration: A Consideration of Oxygen Diffusion Interference. *Biophys. J.* **2006**, *91*, 4623−4631.
(28) Liu, Y.; Imlay, J. A. Cell Death from Antibiotics Without the Involvement of Reactive Oxygen Species. *Science* **2013**, *339*, 1210−1213.
(29) Olczyk, P.; Ramos, P.; Bernas, M.; Komosinska-Vassev, K.; Stojko, J.; Pilawa, B. Microwave Saturation of Complex EPR Spectra and Free Radicals of Burnt Skin Treated with Apitherapeutic Agent. *Evid. Based Complement. Alternat. Med.* **2013**, *2013*, 1.
(30) Alenkina, I. V.; Oshtrakh, M. I.; Klencsár, Z.; Kuzmann, E.; Chukin, A. V.; Semionkin, V. A. 57Fe Mössbauer Spectroscopy and Electron Paramagnetic Resonance Studies of Human Liver Ferritin, Ferrum Lek and Maltofer®. *Spectrochim. Acta, Part A* **2014**, *130*, 24−36.
(31) Jang, H.; Subramanian, S.; Devasahayam, N.; Saito, K.; Matsumoto, S.; Krishna, M. C.; McMillan, A. B. Single Acquisition Quantitative Single-Point Electron Paramagnetic Resonance Imaging. *Magn. Reson. Med.* **2013**, *70*, 1173−1181.
(32) Elas, M.; Williams, B. B.; Parasca, A.; Mailer, C.; Pelizzari, C. A.; Lewis, M. A.; River, J. N.; Karczmar, G. S.; Barth, E. D.; Halpern, H. J. Quantitative Tumor Oxymetric Images From 4D Electron Paramagnetic Resonance Imaging (EPRI): Methodology and Comparison with Blood Oxygen Level-Dependent (BOLD) MRI. *Magn. Reson. Med.* **2003**, *49*, 682−691.
(33) Carocho, M.; Ferreira, I. C. F. R. A Review on Antioxidants, Prooxidants and Related Controversy: Natural and Synthetic Compounds, Screening and Analysis Methodologies and Future Perspectives. *Food Chem. Toxicol.* **2013**, *51*, 15−25.
(34) Mendis, E.; Kim, M.-M.; Rajapakse, N.; Kim, S.-K. An In Vitro Cellular Analysis of The Radical Scavenging Efficacy of Chitooligosaccharides. *Life Sci.* **2007**, *80*, 2118−2127.
(35) Panzella, L.; Gentile, G.; D'Errico, G.; Della Vecchia, N. F.; Errico, M. E.; Napolitano, A.; Carfagna, C.; d'Ischia, M. Atypical Structural and π-Electron Features of a Melanin Polymer That Lead to Superior Free-Radical-Scavenging Properties. *Angew. Chem., Int. Ed.* **2013**, *52*, 12684−12687.
(36) Meinke, M. C.; Friedrich, A.; Tscherch, K.; Haag, S. F.; Darvin, M. E.; Vollert, H.; Groth, N.; Lademann, J.; Rohn, S. Influence of Dietary Carotenoids on Radical Scavenging Capacity of The Skin and Skin Lipids. *Eur. J. Pharm. Biopharm.* **2013**, *84*, 365−373.
(37) Grinolds, M. S.; Hong, S.; Maletinsky, P.; Luan, L.; Lukin, M. D.; Walsworth, R. L.; Yacoby, A. Nanoscale Magnetic Imaging of a Single Electron Spin Under Ambient Conditions. *Nat. Phys.* **2013**, *9*, 215−219.
(38) Le Sage, D.; Arai, K.; Glenn, D. R.; DeVience, S. J.; Pham, L. M.; Rahn-Lee, L.; Lukin, M. D.; Yacoby, A.; Komeili, A.; Walsworth, R. L. Optical Magnetic Imaging of Living Cells. *Nature* **2013**, *496*, 486−489.
(39) Steinert, S.; Ziem, F.; Hall, L. T.; Zappe, A.; Schweikert, M.; Götz, N.; Aird, A.; Balasubramanian, G.; Hollenberg, L.; Wrachtrup, J. Magnetic Spin Imaging Under Ambient Conditions with Sub-Cellular Resolution. *Nat. Commun.* **2013**, *4*, 1607.
(40) Hegyi, A.; Yablonovitch, E. Molecular Imaging by Optically Detected Electron Spin Resonance of Nitrogen-Vacancies in Nanodiamonds. *Nano Lett.* **2013**, *13*, 1173−1178.
(41) Jiang, G.; Jiang, T.; Wang, Y.; Du, X.; Wei, Z.; Zhou, H. Facile Preparation of Novel Au-Polydopamine Nanoparticles Modified by 4-

DOI: 10.1021/acs.jpcb.5b01524
J. Phys. Chem. B 2015, 119, 10341−10347

Mercaptophenylboronic Acid for Use in a Glucose Sensor. *RSC Adv.* **2014**, *4*, 33658−33661.
(42) Della Vecchia, N. F.; Luchini, A.; Napolitano, A.; D'Errico, G.; Vitiello, G.; Szekely, N.; d'Ischia, M.; Paduano, L. Tris Buffer Modulates Polydopamine Growth, Aggregation, and Paramagnetic Properties. *Langmuir* **2014**, *30*, 9811−9818.
(43) d'Ischia, M.; Napolitano, A.; Ball, V.; Chen, C.-T.; Buehler, M. J. Polydopamine and Eumelanin: From Structure−Property Relationships to a Unified Tailoring Strategy. *Acc. Chem. Res.* **2014**, *47*, 3541−3550.
(44) Liu, Y.; Ai, K.; Liu, J.; Deng, M.; He, Y.; Lu, L. Dopamine-Melanin Colloidal Nanospheres: An Efficient Near-Infrared Photothermal Therapeutic Agent for In Vivo Cancer Therapy. *Adv. Mater.* **2013**, *25*, 1353−1359.
(45) Maltempo, M. M.; Eaton, S. S.; Eaton, G. R. Spectral-Spatial Two-Dimensional EPR Imaging. *J. Magn. Reson. (1969-1992)* **1987**, *72*, 449−455.
(46) Eaton, G. R.; Eaton, S. S.; Maltempo, M. M. Three Approaches to Spectral-Spatial EPR imaging. *Int. J. Radiat. Appl.l Instrum. Appl.l Radiat. Isot.* **1989**, *40*, 1227−1231.
(47) Czechowski, T.; Krzyminiewski, R.; Jurga, J.; Chlewicki, W. Two-Dimensional Imaging of Two Types of Radicals by The CW-EPR Method. *J. Magn. Reson.* **2008**, *190*, 52−59.
(48) Blois, M. S.; Zahlan, A. B.; Maling, J. E. Electro Spin Resonance Studies on Melanin. *Biophys. J.* **1964**, *4*, 471−90.
(49) Yordanov, N. D. Quantitative EPR Spectrometry — "State of the art. *Appl. Magn. Reson.* **1994**, *6*, 241−257.
(50) Dyrek, K.; Rokosz, A.; Madej, A. Spin Dosimetry in Catalysis Research. *Appl. Magn. Reson.* **1994**, *6*, 309−332.
(51) Skrzypek, D.; Dzierżęga-Lęcznar, A.; Ziółkowska, J. EPR Investigations of Model Neuromelanins. *Acta Phys. Polym. A* **2000**, *98*, 5661−566.
(52) Cage, B.; Weekley, A.; Brunel, L.-C.; Dalal, N. S. K3CrO8 in K3NbO8 as a Proposed Standard for g-Factor, Spin Concentration, and Field Calibration in High-Field EPR Spectroscopy. *Anal. Chem.* **1999**, *71*, 1951−1957.

DOI: 10.1021/acs.jpcb.5b01524
J. Phys. Chem. B 2015, 119, 10341−10347